Rayleigh–Taylor instability and convective thinning of mechanically thickened lithosphere: effects of non-linear viscosity decreasing exponentially with depth and of horizontal shortening of the layer

Peter Molnar,[1,*] Gregory A. Houseman[2] and Clinton P. Conrad[1]

[1] *Department of Earth, Atmospheric, and Planetary Sciences, Massachusetts Institute of Technology, Cambridge, MA 02139, USA*
[2] *Department of Earth Sciences, Monash University, Clayton, Victoria 3168, Australia*

SUMMARY

Localized mechanical thickening of cold, dense lithosphere should enhance its gravitational instability. Numerical experiments carried out with a layer in which viscosity decreases exponentially with depth, overlying either an inviscid or a viscous half-space, reveal exponential growth, as predicted by linear theory. As shown earlier for a layer with non-linear viscosity and with a constant rheological parameter (Houseman & Molnar 1997), a perturbation to the thickness of the layer grows super-exponentially; for exponential variation of the rheological parameter, the time dependence of growth obeys an equation of the form

$$\left(\frac{Z}{L}\right)^{(1-n)} = (n-1)\left(\frac{C\beta gL^2}{nB_0}\right)^n (t_{\mathrm{b}} - t),$$

where Z is the magnitude of the perturbation to the thickness of the layer; L is the characteristic e-folding distance through the layer for the rheological parameter B, which is proportional to viscosity and reaches a minimum of B_0 at the base of the layer; n is the power relating stress to strain rate; C (~ 0.4, for the experiments considered here) is an empirical constant that depends on wavelength; β is the vertical gradient in density (assumed to decrease linearly with depth in the layer); g is the gravitational acceleration; t is the time; and t_{b} is the time at which a blob of material drawn from the basal part of the layer drops away from the layer. A simple application of this scaling relationship to the Earth, ignoring the retarding effect of diffusion of heat, suggests that somewhat more than half of the lithosphere should be removed in a period of ~ 20 Myr after the thickness of the layer has doubled. The imposition of horizontal shortening of the layer accelerates this process. In the presence of a constant background strain rate, growth will initially be exponential as the non-Newtonian viscosity is governed by the background strain rate. Only after the perturbation has grown to several tens of per cent of the thickness of the layer does growth become super-exponential and yet more rapid. An application of this scaling and its calibration by numerical experiments presented here suggests that super-exponential growth is likely to begin when the perturbation approaches ~ 100 per cent of the thickness of the layer, or roughly 100 km, when applied to the lithosphere. Thus, where the crust has doubled in thickness in a period of 10–30 Myr, we anticipate that roughly half, or more, of the thickened mantle lithosphere will be removed in a period of 10–20 Myr following the initiation of shortening.

Key words: collision belts, lithospheric deformation, mantle convection, mantle rheology, orogeny.

*Also at: Woods Hole Oceanographic Institution, Woods Hole, MA 02543, USA and Laboratoire de Dynamique des Systèmes Géologique, Institut de Physique du Globe de Paris, 4 Place Jussieu 75252 Paris, Cedex 05, France.

1 INTRODUCTION

If, when continental crust thickens during mountain building, the entire lithosphere thickens, then the thickened mantle part of the lithosphere may become gravitationally unstable. Growth of such an instability and the associated removal of part of the mantle lithosphere, which sinks into the asthenosphere, should then perturb the thermal structure of the remaining, overlying lithosphere (Fig. 1). Regional metamorphism, uplift of the overlying surface and changes in the tectonic style of both the uplifted and the surrounding terrains are potential consequences of such an instability (e.g. England & Houseman 1989; Houseman, McKenzie & Molnar 1981; Molnar, England & Martinod 1993; Platt & England 1994). Yet, several aspects of the continental lithosphere might inhibit such an instability, such as the strong temperature dependence of viscosity in the mantle (e.g. Buck & Toksöz 1983; Lenardic & Kaula 1995; Moresi & Lenardic 1997), the non-linear dependence of viscosity on strain rate (Houseman & Molnar 1997) or chemical stratification of the continental lithosphere (e.g. Jordan 1975). To understand how non-linear viscosity might affect such an instability, we have examined its effect on the Rayleigh–Taylor instability, the instability associated solely with a dense layer overlying a denser substrate (Conrad & Molnar 1997; Houseman & Molnar 1997). The present paper is a continuation of these studies.

We focus on two aspects of this instability not considered by Houseman & Molnar (1997). First, we consider the effect of an exponentially decreasing viscosity coefficient through the layer. Our goal was to evaluate the effect of a decrease in viscosity coefficient through the layer on the growth rate and on the amount of the layer removed by the instability. Second, we consider the growth of Rayleigh–Taylor instability in a layer with non-linear viscosity undergoing horizontal shortening. Our objective with these experiments was to understand how such horizontal shortening might alter the temporal development of the instability and accelerate it. One of our main motivations is to demonstrate that the scaling relationships presented by Houseman & Molnar (1997) for non-linear viscosity
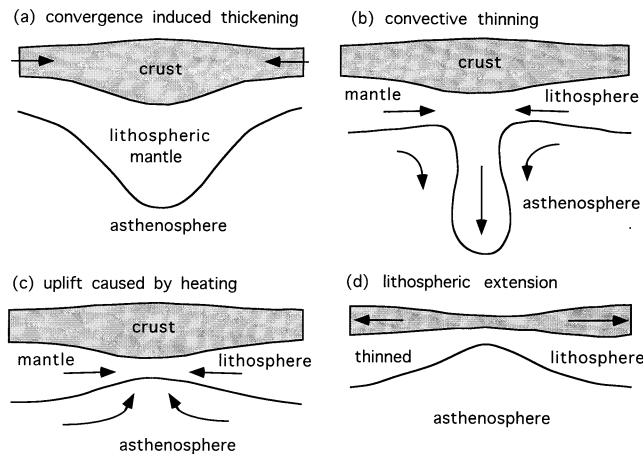

Figure 1. Sequence of four idealized cross-sections showing (a) thickening of both crust and mantle lithosphere, (b) convective instability of the thickened mantle lithosphere and descent of a blob of the lower lithosphere, (c) the resulting thinner mantle lithosphere beneath (at least parts of) the mountain belt and (d) crustal extension and thinning by divergence of the surrounding lithosphere.

can be extended to an exponentially varying rheological coefficient.

Although some form of convective exchange of mass and heat at the base of the lithosphere must occur to supply the heat flux through the plate, few observations constrain the amount of lithosphere likely to be removed by such a process. In regions where thickening of the lithosphere has preceded volcanism, such as Tibet or the Basin and Range Province of the western United States, the volcanic rock carries isotopic and rare-earth signatures that suggest melting of continental lithosphere, not asthenosphere (e.g. Fitton *et al.* 1988; Turner *et al.* 1996). These results imply that neither the entire lithosphere nor only a small fraction of it has been removed. Thus, a second motivation of this paper is to use the scaling laws developed earlier and extended here to estimate the fraction of lithosphere that is likely to be involved in this kind of convective thinning event.

We build on results obtained from linear analysis of the Rayleigh–Taylor instability (Conrad & Molnar 1997) and on simple scaling laws and numerical experiments on finite-amplitude instabilities with both linear (Newtonian) and non-linear viscosity (Houseman & Molnar 1997). For a small perturbation to the base of a dense, constant-viscosity layer over a less dense substrate, the amplitude of the perturbation grows exponentially with time, with a growth rate q (the inverse of the time constant) given by

$$q = \left(\frac{\Delta \rho g h}{2\eta}\right) q'(kh, r) \tag{1}$$

(e.g. Chandrasekhar 1961), where the symbols are defined in Table 1. The function $q'(kh, r)$ describes the dependence of the growth rate on the wavenumber k and the ratio r of the viscosity of the layer to that of the underlying half-space. For a medium in which the viscosity depends on the strain rate the viscosity changes continuously as the perturbation grows, and strain rates respond to the changing viscosity. Where strain rate varies as a power of deviatoric stress, $\dot{\varepsilon} \sim \tau^n$, as has been observed for most rock-forming minerals, we can express the relationship between strain rate and deviatoric stress by

$$\tau_{ij} = B\dot{E}^{(1/n-1)}\dot{\varepsilon}_{ij}. \tag{2}$$

$\dot{E}^2 = (1/2)\Sigma_{i,j}\,\dot{\varepsilon}_{ij}\dot{\varepsilon}_{ij}$ is the second invariant of the strain-rate tensor for an incompressible fluid*. Thus, the viscosity can be written as

$$\eta = \frac{B}{2}\dot{E}^{(1/n-1)}. \tag{3}$$

For the case in which B is constant in the layer, Houseman & Molnar (1997) assumed that the strain rate scales with the ratio of the maximum downward speed (w) of the layer to its thickness (h). This then yielded a simple expression for the growth of the instability:

$$w = \left[C\left(\frac{n-1}{n}\right)\frac{\Delta \rho g}{B}h^{1/n}(t_b - t)\right]^{n/(1-n)}, \tag{4}$$

where C is a dimensionless constant that depends on the wavenumber, the density structure and n; and t_b defines the

* Values of B are defined relative to this definition of the second invariant, which agrees with that of Conrad & Molnar (1997) and is half that of Houseman & Molnar (1997).

Table 1. Definition of symbols.

A	Pre-exponential coefficient in relationship between stress and strain rate
B	Viscosity coefficient (where constant in the layer)
B_0	Viscosity coefficient at the base of the layer, through which it decreases with depth
C	Dimensionless constant that scales growth rates of fluids with non-linear viscosity. Subscripts on C based on timescales T defined in Table 2. Interrelationships of differently defined values of C in Table 3.
$\dot{E}^2$	Second invariant of the strain rate tensor
H	Activation enthalpy in relationship between stress and strain rate
L	Characteristic e-folding depth scale for exponential decrease in viscosity coefficient
R	Universal gas constant
Z	Maximum perturbation to the base of the layer
Z_0	Maximum initial perturbation to the base of the layer
g	Gravitational acceleration
h	Thickness of layer
k	Wavenumber of perturbation to the base of the layer
n	Power relating stress to strain rate
p	Pressure
q	Growth rate of Rayleigh–Taylor instability for Newtonian viscosity. Subscripts on q defined in Table 2.
r	Ratio of the viscosity of the layer to that of the underlying half-space
t	Time
t_b	Time at which the maximum downward speed becomes infinite, and a blob of the basal part of the unstable layer drops away from the remaining part
u_0	Relative convergence rate between the two side boundaries
w	Upward component of velocity of material in or on the boundary of the layer, but used mostly to mean the maximum negative (downward) speed.
x	Horizontal coordinate
z	Vertical coordinate
α	Coefficient of thermal expansion
β	Vertical gradient in density
λ	Wavelength of the initial perturbation to the base of the layer
θ	Temperature
ϑ^2	Second invariant of the stress tensor
$\Delta\rho$	Density difference between the layer and the underlying half-space
η	Newtonian viscosity of the layer ($=B/2$ when $n=1$)
σ_{ij}	Stress component
τ_{ij}	Deviatoric stress component

time when the speed of the materials drawn into the down-welling limb accelerates to infinity, as a blob drops off the bottom of the layer. Integrating eq. (4) yields a time dependence for the maximum displacement of the base of the layer, Z:

$$\left(\frac{Z}{h}\right)^{(1-n)} = (n-1)\left(\frac{C\Delta\rho gh}{nB}\right)^n (t_b - t).\qquad(5)$$

Numerical experiments on a layer overlying an inviscid half-space allowed us to confirm these relationships and to determine the dimensionless constant C and the time t_b as functions of the wavenumber of the perturbation and of n. Canright & Morris (1993) derived a similar time dependence for a layer of constant density and B with stress-free top and bottom boundaries. Moreover, the instability time t_b can be shown to depend on the growth factor C, and on the maximum deflection of the base of the unstable layer at time zero, Z_0 (Houseman

& Molnar 1997):

$$t_b = \left(\frac{nB}{Cg\Delta\rho h}\right)^n \frac{(Z_0/h)^{1-n}}{(n-1)}.\qquad(6)$$

The understanding embodied in eqs (1)–(6) provides the basis for the experiments carried out here.

2 BASIC EQUATIONS AND NON-DIMENSIONALIZATION

The basic equation to be solved is Stokes's equation, which expresses a balance between gradients in stress and body forces, when inertial terms can be neglected:

$$\frac{\partial \sigma_{ij}}{\partial x_j} - \rho g \delta_{iz} = 0,\qquad(7)$$

where σ_{ij} is the stress component and δ_{ij} is the Kronecker delta. The stress components are separated into isotropic (p) and deviatoric (τ_{ij}) parts:

$$\sigma_{ij} = p\delta_{ij} + \tau_{ij},\qquad(8)$$

where eqs (2) and (3) relate τ_{ij} to the strain rate. We assume that the flow field induced in the layer is incompressible:

$$\dot{\varepsilon}_{ii} = \frac{\partial u_i}{\partial x_i} = 0.\qquad(9)$$

Although we neglect accelerations in the balance of forces, time dependence appears because gravity acts on any small perturbation to the flat base of the heavier, overlying layer and induces a flow field, which, in turn, amplifies the perturbation at a rate whose magnitude depends on the size of the perturbation. Growth manifests itself most clearly by the time evolution of the position of the base of the layer.

The layer is bounded by its basal free surface $S(x, z)$, initially at $z = 0$, and its upper rigid surface at $z = h$. Gravity acts in the negative z direction and the rheological parameter that governs viscosity, B, decreases exponentially with depth, with a scaling length L, through a layer of thickness h (Fig. 2):

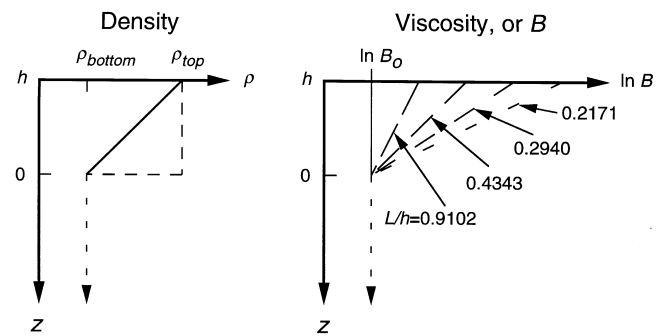$$B(z) = B_0 \exp(z/L), \quad 0 \le z \le h.\qquad(10)$$

Figure 2. Simple cross-sections of density (left) and $\ln B$ (right) for the experiments. We use two density structures within a layer of thickness h, the density in one case being constant within the layer, and in the other case linearly decreasing, both overlying a layer of constant density. For rheological structures, in most cases, the rheological parameter B decreases with depth exponentially, and in most cases the underlying structure is inviscid. For cases with a viscous substrate, the viscosity is equal to that at the base of the layer.

Because we ignore inertial terms, magnitudes of density are unimportant; only variations in density matter. We consider two possible density distributions: constant density,

$$\Delta\rho = \rho_{\text{top}} - \rho_{\text{bottom}} = \text{constant}, \quad 0 \le z \le h, \tag{11}$$

and linearly decreasing density,

$$\rho(z) = (\rho_{\text{top}} - \rho_{\text{bottom}})z/h = \beta z, \quad 0 \le z \le h, \tag{12}$$

with $\rho(z) = \rho_{\text{bottom}}$ for $z \le 0$ for both. In either case, the density is relative to an assumed constant-density lower layer. Both the density and the viscosity coefficient are considered to be material properties of the fluid and are advected with the flow.

We carried out a series of numerical experiments using the same finite element code as Houseman & Molnar (1997). For most cases, meshes were constructed with ~ 5000 nodes forming a mesh of approximately equilateral triangles. Quadratic interpolation was used for the velocity field and linear interpolation for pressure. Time stepping was done by a second-order Runge–Kutta integration in which node points were advected by the flow field in order to compute the motion of the free surface at the base of the layer.

We examined the dependence of growth rates on the wavenumber of a sinusoidal perturbation of fixed wavelength λ ($=2\pi/k$) by setting the width of the layer equal to $\lambda/2$, and by perturbing the lower surface of the layer at $t = 0$ by

$$S(x, z) = \{x, -Z_0 \cos(2\pi x/\lambda)\}. \tag{13}$$

We experimented with the amplitude of the perturbation and commonly used $Z_0 = 0.01h$, $0.001h$ or $0.0001h$.

For boundary conditions we permitted no movement at the top of the layer, $z = h$, and allowed the two sides, at $x = 0$ and $x = \lambda/2$, to slide vertically, but not horizontally. For shear stress on those sides we set $\tau_{xz} = 0$. We generally assumed a lower layer of constant density (zero in the reference frame used for density) whose viscosity was small compared to the upper layer. Under these conditions, the tractions on the lower boundary of the layer are zero throughout the growth of the instability ($\sigma_{xz} = 0$ and $\sigma_{zz} = 0$) regardless of the shape of the boundary. For some experiments we included a lower layer of constant properties in which the flow was explicitly calculated, assuming that displacements and tractions were continuous across the boundary.

Although two scaling dimensions, L and h, are generally present, linear analysis indicates, at least for media with Newtonian viscosity, that for a viscosity variation across the layer of order 10 or more, the more important dimension is that governing viscosity (Conrad & Molnar 1997). Thus we define the dimensionless length parameters

$$(x', y') = (x, y)/L \tag{14}$$

except where B is constant throughout the layer ($L \to \infty$). For this case

$$(x', y') = (x, y)/h. \tag{15}$$

The choice of scale for the dimensionalization of time follows from the growth rate defined by eq. (1), but is modified by Houseman & Molnar (1997) for a non-Newtonian fluid and generalized here for application to a layer with stratified density and viscosity by substitution of the length scale L. Thus $t' = t/T_{L\beta}$, where

$$T_{L\beta} = \left(\frac{B_0}{g\beta L^2}\right)^n, \tag{16}$$

and the subscript $L\beta$ distinguishes this scaling from those where different length and density scales are used. In particular, we use h in place of L if $L \to \infty$, and if $\beta = 0$ (constant-density layer) we use $\Delta\rho$ in place of βL. For Newtonian viscosity ($n = 1$), $B_0 = 2\eta_0$. The range of experiments studied here requires that we use a number of distinct dimensionalization schemes, as listed in Table 2.

3 RESULTS WITH EXPONENTIALLY DECREASING NEWTONIAN VISCOSITY

For Newtonian viscosity, we may calculate theoretical growth rates during the initial growth, when non-linear terms in the basic equations are small. Following Conrad & Molnar (1997), we use propagator matrix methods developed by Bassi & Bonnin (1988) to determine growth rates linearized about a basic background state of pure shear. This analysis is also applicable for Newtonian rheology and zero background strain rates (Conrad & Molnar 1997). These linearized growth rates are compared with those determined from the 2-D non-linear calculations to verify the accuracy of the two computational methods and to extend the range of wavenumbers studied experimentally.

3.1 Constant density in a layer overlying an inviscid half-space

We carried out experiments with viscosity varying across the layer by 3, 10, 30 and 100 times, corresponding to $L = 0.9102h$, $0.4343h$, $0.2940h$ and $0.2171h$ respectively in eq. (10). Lengths are rendered dimensionless using L, and times using $T_{L\Delta\rho} = 2\eta_0/(\Delta\rho gL)$ (Table 2). Because we expect that perturbations initially will grow exponentially, we plot logarithms of the downward speed w' and of Z', the vertical coordinate of the bottom left corner of the mesh, against dimensionless time. In general, this corner of the layer, where the perturbation is maximum, moves most rapidly and farthest as the perturbation grows. For both w' and Z', we fitted straight lines of the form

$$\ln w' = \ln w'_0 + q'_{\text{est}} t' \tag{17}$$

to the initial straight-line segments of the data, and we estimated q'_{est} for each* (Fig. 3). The growth rates determined from these experiments (shown as solid lines, the best fit to the early part of the curves, in Fig. 3) agree within a few per cent with those predicted by the linearized theory (Fig. 4). In general, growth rates determined from Z' fit the linearized theory better than those based on w'. When some of these calculations were repeated with a denser mesh we found agreement of measured growth rates to four figures, suggesting that the disagreement between the two calculation methods is probably explained mainly by the discretization error in the finite-element method.

Plots of dimensionless growth rates as a function of dimensionless wavenumber k' yield curves (Fig. 4) with maxima that depend only on the length scale of viscosity variation, L/h. Growth rates for variations in viscosity of 30 times ($L/h = 0.2940$), 100 times ($L/h = 0.2171$) and higher differ little. The maximum dimensionless growth rate in the limit of small L is $q'_L \approx 0.28$ for $k' \approx 1$ ($\lambda \approx 2\pi L$). In the opposite limit

*Information regarding the location of experimental data is available from the Royal Astronomical Society (vjd@ras.org.uk).

Table 2. Dimensionless growth rates or growth constants and their defining dimensionless timescales.

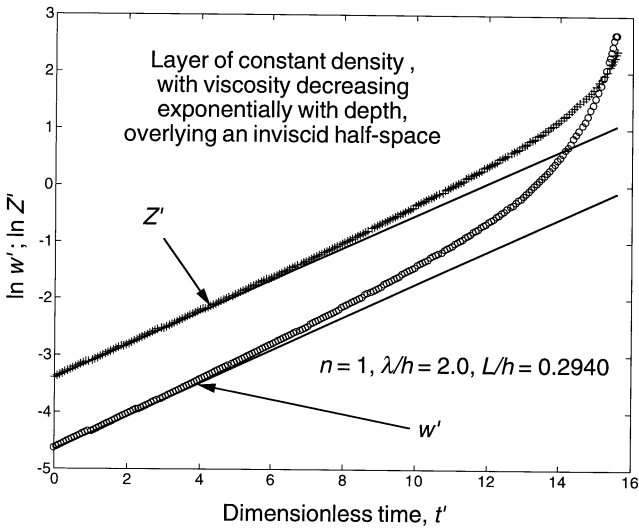| Dimensionless growth rate	Scale for distance	Scale for density	Defining timescale	Defining equation number
$q'_h = qT_{h\Delta\rho}$	h	$\Delta\rho$	$T_{h\Delta\rho} = \dfrac{2\eta}{\Delta\rho gh}$	(1)
$q'_L = qT_{L\Delta\rho}$	L	$\Delta\rho$	$T_{L\Delta\rho} = \dfrac{2\eta_0}{\Delta\rho gL}$	
$q'_L = qT_{L\beta}$	L	βL	$T_{L\beta} = \dfrac{2\eta_0}{g\beta L^2}$	(16)
$q''_h = qT_{hs}$	h	βh	$T_{hs} = \left(\dfrac{B}{g\beta h^2}\right)\left(\dfrac{2u_0}{\lambda}\right)^{(1-n)/n}$	(28)
$q''_L = qT_{Ls}$	L	βL	$T_{Ls} = \left(\dfrac{B}{g\beta L^2}\right)\left(\dfrac{2u_0}{\lambda}\right)^{(1-n)/n}$	
$C_{h\Delta\rho}$	h	$\Delta\rho$	$T_{h\Delta\rho} = \left(\dfrac{B}{g\Delta\rho h}\right)^n$	
$C_{L\Delta\rho}$	L	$\Delta\rho$	$T_{L\Delta\rho} = \left(\dfrac{B_0}{g\Delta\rho L}\right)^n$	
$C_{h\beta}$	h	βh	$T_{h\beta} = \left(\dfrac{B}{g\beta h^2}\right)^n$	(16)
$C_{L\beta}$	L	βL	$T_{L\beta} = \left(\dfrac{B_0}{g\beta L^2}\right)^n$	

Figure 3. Examples of $\ln w'$ and $\ln Z'$ plotted versus t' for a layer with constant density and with Newtonian viscosity, $n = 1$ in eq. (3), decreasing exponentially with depth in the layer, which, in turn, overlies an inviscid half-space. The linearity of the initial data defines the growth rate q'_L, which has been rendered dimensionless using $T_{L\Delta\rho}$ (Table 2).

of a constant-viscosity layer ($L \gg h$), Houseman & Molnar (1997) obtained q'_h ($= 2\eta q/\Delta\rho gh$) $\rightarrow 0.32$ at a wavenumber k' ($= 2\pi h/\lambda$) ≈ 2.12.

3.2 Density decreasing linearly with depth, inviscid substrate

Similar calculations for a density decreasing linearly with depth through the layer yield similar patterns (Fig. 5).
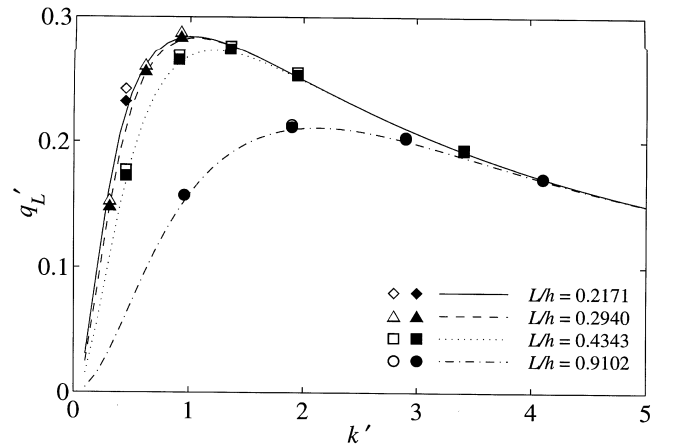

Figure 4. Plot of measured (symbols) and theoretical (lines) growth rates q'_L versus wavenumber k', for a layer of constant density and with viscosity decreasing exponentially with depth, overlying an inviscid half-space. Values shown by open symbols are based on measurements of downward speeds of the bottom left corner of the layer and values shown by solid symbols are based on displacements of it. Note that as L/h decreases, the dependence of $q'_L(k')$ on L/h also decreases.

Again, perturbations initially grow exponentially. Moreover, measured growth rates, here rendered dimensionless using $T_{L\beta} = 2\eta_0/(\beta g L^2)$ (Table 2), again differ from those predicted by the linearized theory by less than a few per cent. As the ratio L/h becomes small and the variation in viscosity becomes large, the dimensionless growth rate tends to a maximum $q'_{max} \approx 0.210$ at a wavenumber $k'_{max} \sim 0.8$.

Growth for a linear density is slower than for a constant density. Compared to a reference case of constant viscosity, the dimensional growth rate for a constant-density layer is
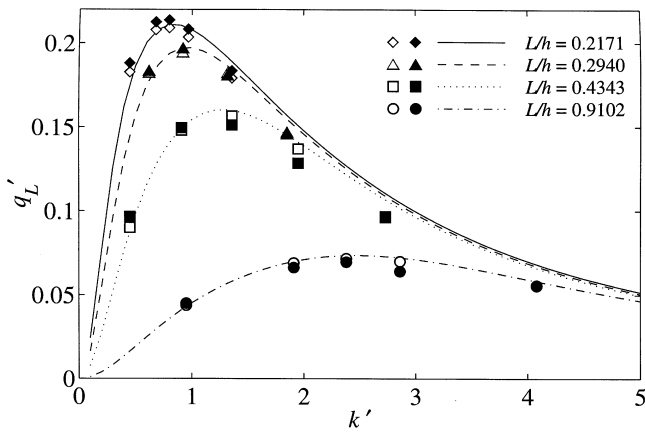
Figure 5. Plot of measured (symbols) and theoretical (lines) growth rates q'_L versus wavenumber k', for a layer with density decreasing linearly and viscosity decreasing exponentially with depth, overlying an inviscid half-space. As in Fig. 4, the values shown by open symbols are based on measurements of downward speeds of the bottom left corner of the layer and the values shown by solid symbols are based on displacements of it. Again as in Fig. 4, for small values of L/h the dependence of $q'_L(k')$ on L/h decreases.

proportional to L/h, but the rate for a linearly decreasing density scales as $(L/h)^2$. For small L/h, the dimensional growth rate for a linearly increasing density is smaller by a factor of approximately $0.75(L/h)$ than that for constant density (compare Figs 4 and 5). For large L/h (constant viscosity), however, this ratio of growth rates approaches 0.38 (Houseman & Molnar 1997). Recall that the total mass anomaly in the linear-density layer is only half of that in the constant-density layer, by eqs (11) and (12). More importantly, for constant density, the most unstable part of the layer is near its base, where the density contrast is high and the viscosity is lowest. With linearly decreasing density, the density anomaly vanishes at the base of the layer, and the unstable mass is centred higher in the layer, where the viscosity is higher than at the base. Thus, a greater thickness of the layer should be involved in the instability when density decreases linearly (Houseman & Molnar 1997).

3.3 Density decreasing linearly with depth, viscous substrate

An advantage of a layer with exponentially decreasing viscosity overlying an inviscid half-space is that calculations can be made quickly, without the need for calculating flow in the underlying half-space. Although a layer over an inviscid half-space at first appears to provide a poor model of the Earth, studying such a structure is justified if the inclusion of an underlying viscous fluid has, at most, a small effect on growth rates. As a test, we constructed a two-layered medium by adding a thick lower layer whose (Newtonian) viscosity was set equal to that at the base of the upper layer, i.e. $B(z) = B_0$ for $z < 0$, and whose density was constant and equal to the density at the base of the upper layer. We used lower layers four times as thick as the upper layers, after finding that the base of such a layer was deep enough that its behaviour approximates that of a half-space. The density of finite-element node points in the lower layer decreases with depth, but with similar resolution near the interface of the layers. The shape
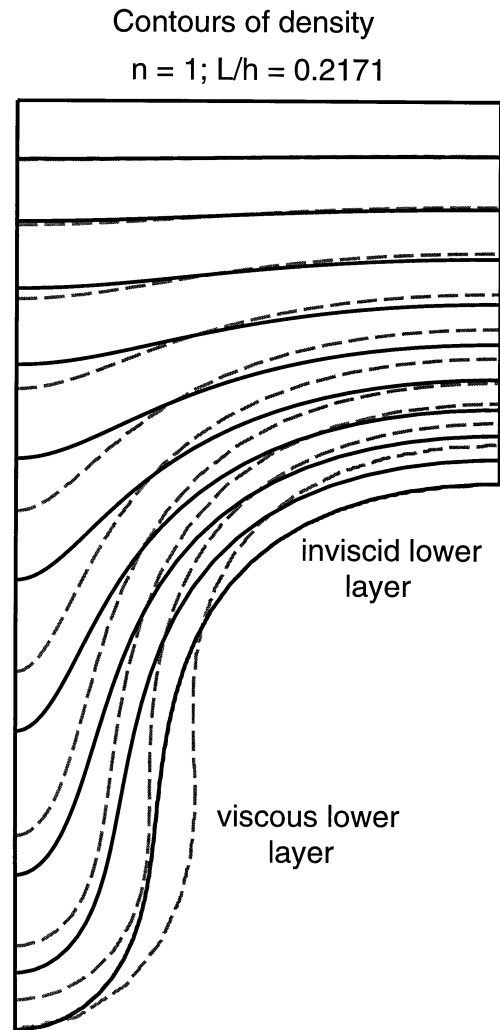
Contours of density
n = 1; L/h = 0.2171

Figure 6. Contours of density within the upper layer for two experiments in which $n = 1$, $\lambda/h = 1.7$, density decreases linearly with depth, viscosity decreases exponentially with depth and either the layer overlies an inviscid half-space (solid lines) or the layer overlies another layer of depth $4h$, with density and viscosity equal to those at the base of the upper layer (dashed lines). Contours at increments of $0.1\Delta\rho$ are shown and the lowermost contour is coincident with the base of the upper layer ($\Delta\rho = 0$). The instability clearly grows faster when the lower layer is inviscid; this comparison shows two experiments when the lower left corner has sunk to $z = -0.628h$, at times of $t' = 18.9$ and $t' = 23.9$ respectively.

of the base of the layer in contact with a viscous substrate differs little from that over an inviscid fluid (Fig. 6).

We calculated dimensionless growth rates as a function of k' for a layer with density decreasing linearly with depth over a half-space (Fig. 7), using the linearized procedures described by Conrad & Molnar (1997), and we then carried out the full finite element calculations with the two-layered mesh for wavenumbers close to k'_{max}. Again the experimental values of q'_L agree within a few per cent with those calculated from the linearized theory (Fig. 7). The functional dependences of $q'_L(k')$ for a layer over an inviscid half-space (Fig. 5) and over a viscous half-space (Fig. 7) differ little, especially for small ratios of L/h, corresponding to rapid decreases in viscosity with depth in the layer. For viscosity variations of 100
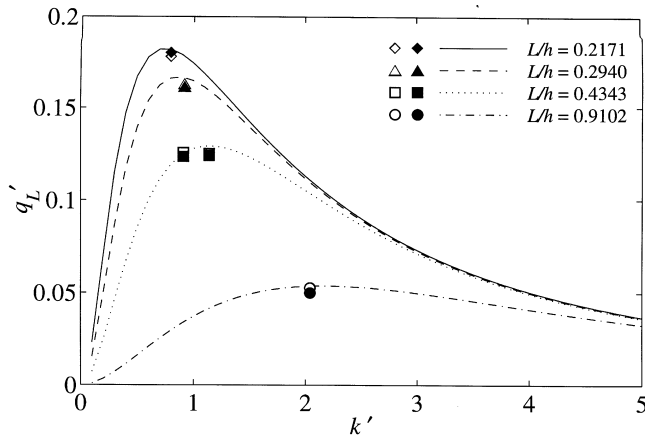
Figure 7. Plot of growth rates q'_L versus wavenumber k' from finite element (symbols) and linearized (lines) calculations for a layer with density decreasing linearly and viscosity decreasing exponentially with depth, overlying a deep layer with constant density and viscosity equal to those at the base of the top layer. Open and solid symbols as in Fig. 4. As in Fig. 4, for small values of L/h the dependence of $q'_L(k')$ on L/h decreases.

($L/h = 0.2171$), for instance, the value of q'_{max} for an unstable layer falling into a viscous substrate is only ~ 15 per cent smaller than that for an inviscid substrate.

3.4 Summary of results: exponentially decreasing Newtonian viscosity

The results summarized in Figs 4, 5 and 7 show, first, that calculations of finite-amplitude growth of the Rayleigh–Taylor instabilities match the predictions of the linearized theory for initial, small-amplitude growth. One may view this agreement as confirmation that the finite-amplitude program gives accurate results. Second, both calculations show that as L/h decreases (and viscosity decreases rapidly through the layer), both k'_{max} and q_{max} become independent of that ratio. Thus, results for moderate values of L/h (less than about 0.3) may be used for drawing inferences appropriate for small values of that ratio. Perhaps most important, however, is the demonstration that exclusion of a viscous substrate does not affect growth rates much. Thus, little understanding is gained by making laborious, realistic calculations with a viscous substrate.

4 RESULTS WITH EXPONENTIALLY DECREASING NON-LINEAR VISCOSITY COEFFICIENT

We carried out a similar series of experiments for a layer whose non-linear viscosity is given by eq. (3) with $n = 3$, and a depth-dependent coefficient B defined by eq. (10), for (1) a layer with constant density over an inviscid half-space, (2) a layer with density decreasing linearly through it over an inviscid half-space and (3) a layer with density decreasing linearly through it over a viscous half-space, with the rheological parameter matching that at the base of the upper layer. Again the purpose was to quantify how an exponential variation in the rheological parameter B affects growth. Linearized calculations cannot be made for $n = 3$, because the power-law growth of the instability

means that the solution depends on the reference viscosity about which the equations are linearized.

4.1 Constant density in a layer overlying an inviscid half-space

As for Newtonian viscosity, we carried out experiments with vertical variations in B of 3, 10, 30 and 100 times across the layer. We tested the assumption that growth would follow forms similar to those of eqs (4) and (5), derived by Houseman & Molnar (1997). In our previous analysis of the layer with constant B (Houseman & Molnar 1997), we showed a simple, general form of the instability by making eqs (4), (5) and (6) dimensionless using the length scale h, the thickness of the layer. In what follows we show that, for B decreasing exponentially, a similarly simple form results from making the equations dimensionless using the length scale L. We then compare the results of these two sets of experiments in order to describe the effect of decreasing L on the growth time of the instability.

Non-dimensionalizing eqs (4) and (5), using $\Delta\rho h$ in place of βL^2 in eq. (16), yields

$$w' = \left[C_{h\Delta\rho} \left(\frac{n-1}{n} \right) (t'_b - t') \right]^{n/(1-n)}, \tag{18}$$

$$Z'^{(1-n)} = (n-1) \left(\frac{C_{h\Delta\rho}}{n} \right)^n (t'_b - t'). \tag{19}$$

Again, the subscript $h\Delta\rho$ indicates the length and density scales used in the non-dimensionalization. The dimensionless parameter $C_{h\Delta\rho}$ [$=C$, in eqs (4)–(6)] quantifies the rate at which the instability grows. Houseman & Molnar (1997) tested eqs (18) and (19) by plotting Z'^{1-n} and $w'^{(1/n-1)}$ versus t' and estimated $C_{h\Delta\rho}$ appropriate for the limit $L/h \to \infty$.

Assuming that the basic physics that led to such relationships applies also to the case of viscosity decreasing exponentially with depth, we also plotted Z'^{1-n} and $w'^{1/n-1}$ versus t', but now using the dimensionalization based on L (eq. 16) for $L/h < 1$, and approaching $L/h \ll 1$. Again the data define straight lines (Fig. 8), which allow us to determine values of $C_{L\Delta\rho}(k', n, L/h)$ (Fig. 9). Because of the different dimensionalizations of $C_{L\Delta\rho}$ and $C_{h\Delta\rho}$, however, as $L/h \to 0$, $C_{h\Delta\rho}$ becomes an inappropriate measure of the growth rate, as does $C_{L\Delta\rho}$ when $L/h \to \infty$, as shown by eq. (III.1) in Table 3.

As found for constant B, the values of $C_{L\Delta\rho}$ inferred from analyses of time series of w' and Z' differ by a few per cent. We infer this to reflect a combination of experimental errors as well as errors in eqs (18) and (19), since these equations, like eqs (4) and (5), are only approximations, not rigorously derived. Because we treat values of C, in general, as accurate to only one, or at most two, significant figures, these differences do not concern us here. $C_{L\Delta\rho}$ depends only weakly on L for $L/h < 0.43$ (Fig. 9). This dependence reveals that, for exponential variations in B, k'_{max} is shifted towards larger values, or shorter wavelengths, than for Newtonian viscosity (Fig. 4). Like q'_L for Newtonian viscosity, $C_{L\Delta\rho}$ becomes independent of L/h for small values of L/h; we observe a weaker dependence on L/h for $C_{L\Delta\rho}$ with $n = 3$ than for q'_L with $n = 1$. Because the effective viscosity, which depends on strain rate, increases much more rapidly with height for $n = 3$, even experiments with $L/h = 0.4343$ are well into the asymptotic domain in which the only important length scale is L.
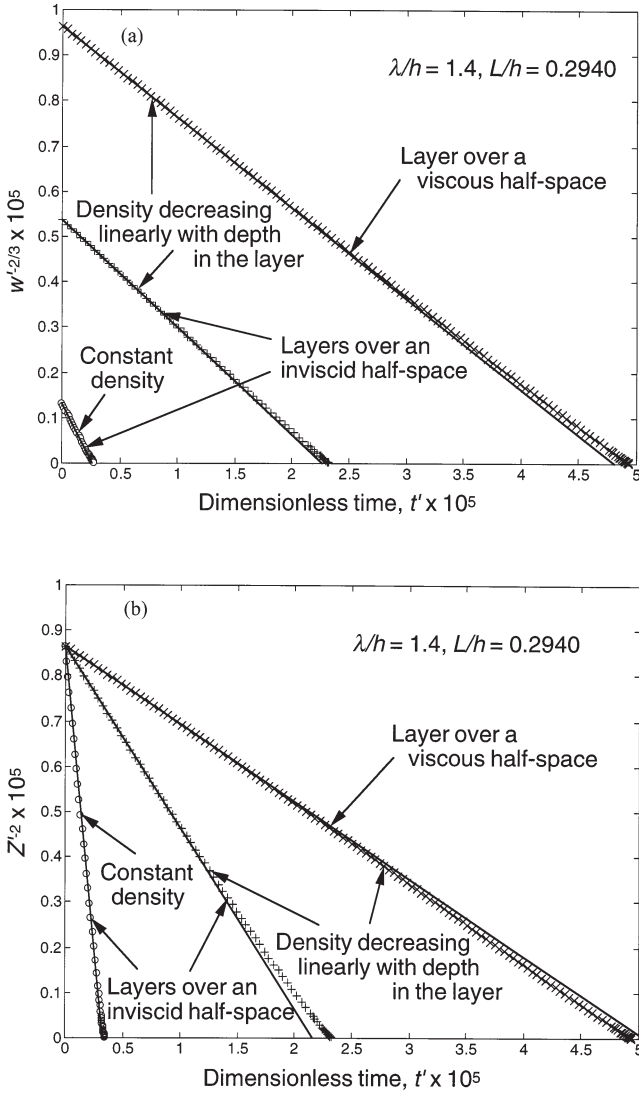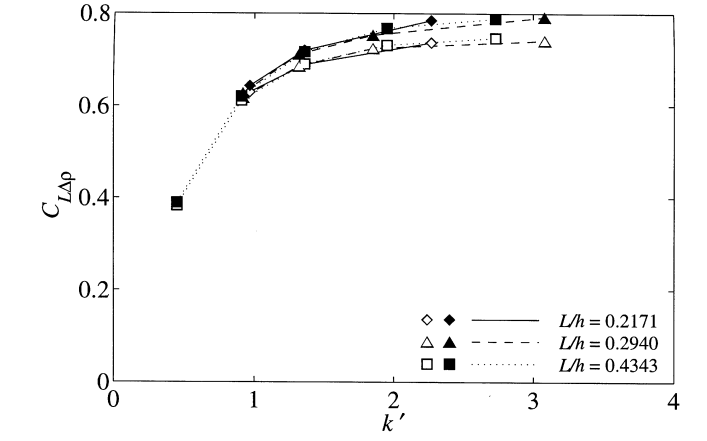
Figure 9. Measured values of $C_{L\Delta\rho}$ plotted against k' for a layer of constant density and constant rheological exponent $n = 3$ in eq. (3), with the rheological parameter B decreasing exponentially with depth in a layer overlying an inviscid half-space. Open and solid symbols as in Fig. 4. As for the runs with Newtonian viscosity, the values of $C_{L\Delta\rho}$ depend only weakly on the ratio L/h when it is sufficiently small.

The maximum values of $C_{L\Delta\rho}$ (≈ 0.76) as $L/h \to 0$ differ only slightly from those for constant viscosity, $C_{h\Delta\rho} \approx 1.1$, corresponding to $L/h \to \infty$ (Houseman & Molnar 1997). Because of the different dimensionalization schemes (Table 3, eq. III.1), however, this similarity could be misleading. The simplest way to describe the impact of the viscous strength coefficient increasing upwards is to compare the dimensional instability time (eq. 6) for experiments that differ only in the value of L, with each having the same viscosity coefficient at the base of the layer (Table 3, eq. III.2). For example, the actual timescale of the instability is increased by a factor of ~ 7 as L/h is decreased from ∞ to 0.4343 with $n = 3$. For smaller values of L/h the instability time increases in inverse proportion to L/h.

4.2 Density decreasing linearly with depth, inviscid substrate

We made similar calculations with the density decreasing linearly with depth in the layer, again overlying an inviscid half-space. The density gradient β is defined by $\beta = \Delta\rho/h$. As before, plots of Z'^{1-n} and $w'^{(1/n-1)}$ versus t', with times non-dimensionalized by eq. (16), lengths by L and densities by βL, yield straight lines (Fig. 8) whose slopes determine the growth coefficients $C_{L\beta}$ (Fig. 10). Like $C_{L\Delta\rho}$ (Fig. 9), $C_{L\beta}$ depends only weakly on L for experiments with linearly decreasing density (Fig. 10). The wavenumber dependence of $C_{L\beta}$ shows maximum

Figure 8. Examples of (a) $w'^{1/n-1}$ and (b) Z'^{1-n} plotted versus t' for three runs, all with $n = 3$, $\lambda/h = 1.4$ and $L/h = 0.2940$. In both (a) and (b), the central time-series (+) shows results for a layer with density decreasing linearly with depth, overlying an inviscid half-space. The upper time-series (×) shows results for a layer over a viscous half-space. In these cases, times are non-dimensionalized by eq. (16). The lower left time-series (○) shows results for a layer of constant density over an inviscid half-space, for which times are non-dimensionalized by eq. (16), but with $\beta L = \Delta\rho$. The lines fit to these data yield estimates of the dimensionless parameter C via eqs (18) and (19). Notice that growth is faster for a layer of constant density than for a layer with density decreasing with depth, and faster for a layer over an inviscid half-space than over a viscous half-space.

Table 3. Relationships between dimensionless growth constants defined in Table 2 (left-hand columns) and ratios of instability times (right-hand columns) derived from those growth factors using eq. (16).

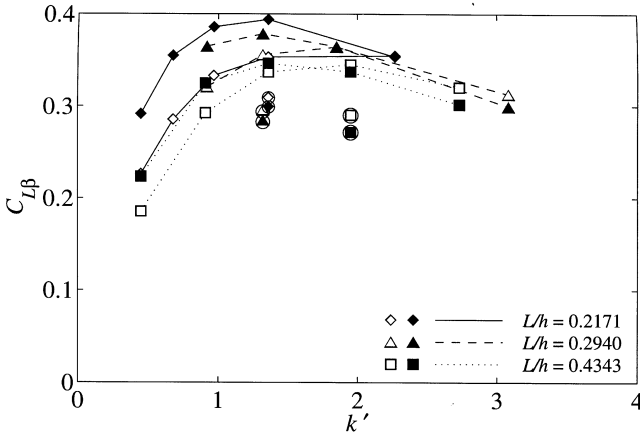|			
$C_{L\Delta\rho} = \left(\dfrac{h}{L}\right)^{1/n} C_{h\Delta\rho}$	(III.1)	$\dfrac{t_b(\Delta\rho, L)}{t_b(\Delta\rho, L \to \infty)} = \dfrac{h}{L}\left(\dfrac{C_{h\Delta\rho}(L \to \infty)}{C_{L\Delta\rho}(L)}\right)^n$	(III.2)
$C_{L\beta} = \dfrac{h}{L} C_{L\Delta\rho}$	(III.3)	$\dfrac{t_b(\beta, L)}{t_b(\Delta\rho, L)} = \left(\dfrac{L}{h}\right)^{-n}\left(\dfrac{C_{L\Delta\rho}(L)}{C_{L\beta}(L)}\right)^n$	(III.4)
$C_{h\beta} = \left(\dfrac{L}{h}\right)^{(n+1)/n} C_{L\beta}$	(III.5)	$\dfrac{t_b(\beta, L)}{t_b(\beta, L \to \infty)} = \left(\dfrac{L}{h}\right)^{-(n+1)}\left(\dfrac{C_{h\beta}(L \to \infty)}{C_{L\beta}(L)}\right)^n$	(III.6)

Figure 10. Plot of measured values of $C_{L\beta}$ versus k' for density decreasing linearly, constant rheological exponent $n = 3$ in eq. (3) and viscosity decreasing exponentially with depth in layers either overlying an inviscid half-space (regular symbols) or overlying a viscous half-space (circled symbols), with the rheological parameter in the half-space equal to B_0. Open and solid symbols as in Fig. 4. Although the values of $C_{L\beta}$ for such a density structure differ from those for constant density (Fig. 9), the values again depend only weakly on the ratio L/h when it is sufficiently small. Moreover, as for Newtonian viscosity (Fig. 7), the effect of adding a viscous substrate is to retard growth of the instability, but values of $C_{L\beta}$ differ from those for an inviscid substrate by only ~ 20 per cent.

values between 0.3 and 0.4, at wavenumbers $k' = Lk$ of approximately 1.5. The ratio $C_{L\beta}/C_{L\Delta\rho}$ is similar to the ratio $C_{h\beta}/C_{h\Delta\rho}$ for layers with constant B (Houseman & Molnar 1997).

The time for the instability to occur in a layer of linearly decreasing density is increased by the factor $(L/h)^{-n}(C_{L\Delta\rho}/C_{L\beta})^n$ relative to that for a constant-density layer with the same viscosity profile (Table 3, eq. III.4), a factor that is of order 100 for $n = 3$ and $L/h = 0.4343$. By comparison, Houseman & Molnar (1997) found for a constant viscosity coefficient $(L \to \infty)$ that the instability time for a linearly decreasing density is a factor of about 16 times greater than that for constant density*. Using Houseman & Molnar's (1997) maximum value of $C_{h\beta}(L \to \infty) \approx 0.47$, our value of $C_{L\beta}(L) \approx 0.35$, $n = 3$ and eq. (III.6) of Table 3, the instability time for $L/h = 0.4343$ is approximately 68 times greater than that for the same experiment with $L \to \infty$. As the maximum values of $C_{L\beta}$ are almost constant for small L/h, decreasing L/h causes the instability time to increase in proportion to $(L/h)^{-(n+1)}$, with other factors constant. As the latter statement holds also for $n = 1$, as shown above in Section 3.2, a similar decrease in L has a greater impact for $n = 3$ than for $n = 1$.

Like the growth rates for $n = 1$, the maximum values of $C_{L\beta}$ for linearly decreasing density are reached at smaller wavenumbers k'_{max} than they are for constant density. For instance, for constant density and $L/h = 0.2171$, $k'_{max} > 2$ (Fig. 9), but for a density increasing linearly, k'_{max} is close to 1.5 (Fig. 10).

4.3 Density decreasing linearly with depth, viscous substrate

As for Newtonian viscosity, we added a lower layer four times as thick as the upper denser layer, in order to simulate a half-

---

*Houseman & Molnar (1997) quoted values of $C_{h\beta}$ for the case in which $\beta = 2\Delta\rho/h$. We remove the factor of 2 here.

space beneath the layer. We assigned values of the rheological parameter B and the density ρ in the lower layer equal to the corresponding values at the base of the upper layer and assumed $n = 3$ in both layers. Our purpose was merely to examine how $C_{L\beta}$ depended on the presence of the lower layer. We calculated the growth of the instability for values of k' near k'_{max} (Figs 8 and 10). As for Newtonian viscosity, the presence of the viscous substrate retards growth but not very much. Values of $C_{L\beta}$ with the viscous substrate are less than those of the counterpart runs with an inviscid substrate by between a few per cent and about 20 per cent, resulting in an increase in the instability time of between 10 per cent and 100 per cent for $n = 3$.

4.4 Thickness of layer removed by instability

Because the layer is heavier than the underlying half-space, after an infinite amount of time almost the entire layer will be removed. In the period that elapses during our experiments, however, the basal portion of the layer thins, as it is drawn into the downwelling limb, and only the bottom of the layer, where the rheological parameter B (or viscosity) is lowest, is removed. As time passes further, this basal portion will continue to thin but at a rate that is reduced, because its average viscosity increases.

From the experiments, we may estimate the amount of thinning after a period of approximately t_b. If the growth of the instability followed the theoretical relationship given by eq. (19), we could simply extrapolate the results and use the thickness of the layer at $x = \lambda/2$ and $t = t_b$ to estimate the thickness Δh of material removed. Because of deviations of Z'^{-2} from eq. (19) at times near $t = t_b$, however, this does not yield a reliable estimate of the thickness of material removed. In some cases, Z'^{-2} approaches zero at times slightly later than $t = t_b$, but for others, it does so for times slightly earlier than $t = t_b$ (Fig. 8). Thus, we first extrapolated Z'^{-2} for the last two time steps to obtain an estimate of time at which $Z'^{-2} = 0$. Then, we extrapolated the thickness of the thinned side of the layer to that time to estimate Δh.

For layers over an inviscid half-space, values of Δh are commonly in the range 0.7–$0.9L$ (Fig. 11a), but for layers over a viscous half-space, $\Delta h > L$. The reason for this difference is not obvious, but presumably circulation in the viscous substrate, generated by the high-density blob, applies stress to the base of the upper layer. In any case, it appears that the maximum thickness of material effectively removed by the initial growth of the instability in a time t_b is $\Delta h \sim L$ (Fig. 11a).

To estimate how much of the layer is removed after a greater time interval, we must exploit the understanding already gained, for the finite-element algorithm cannot handle the distortion associated with removal of the basal layer without extensive regridding of the mesh. We first turn the question around and ask what time period t_p is required to remove the thickness $\Delta h = pL$. The following argument, using a layer of constant density as an example, is only approximate. If $p = 1$ then, from Fig. 11(a),

$$t_p \approx t_b = \frac{(Z_0/L)^{1-n}}{(n-1)}\left(\frac{nB_0}{C_{L\Delta\rho}g\Delta\rho L}\right)^n. \tag{20}$$

If $p = 2$, the next increment in Δh is removed in a time that may be estimated assuming $Z_0 \approx L$ and increasing B_0 by the factor e. Succeeding increments may be calculated in the same
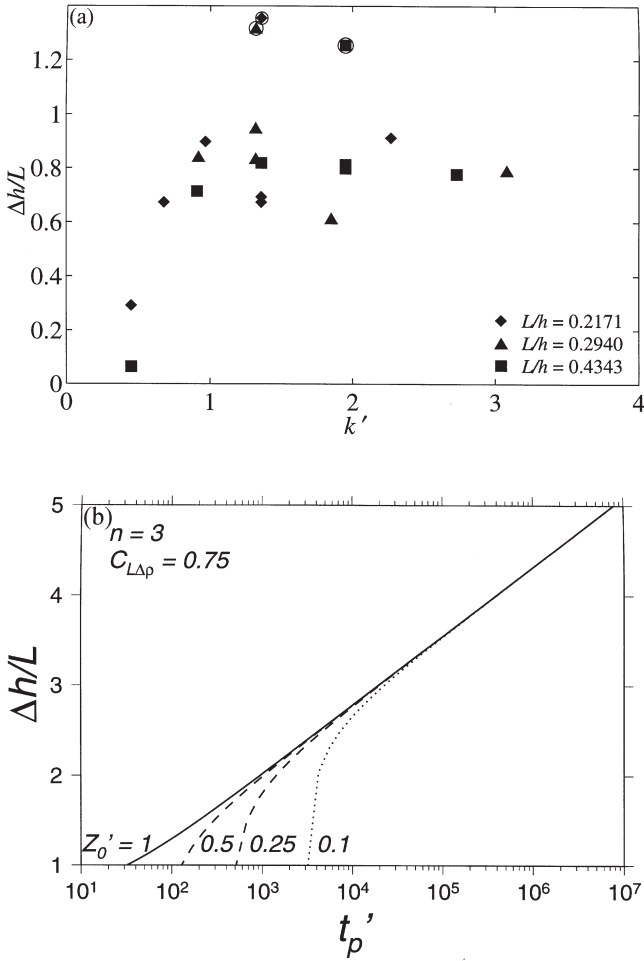
Figure 11. (a) Estimated thickness of the layer $\Delta h/L$ removed in time $t' \approx t'_b$ during the initial instability and (b) extrapolated thickness $\Delta h/L$ removed after time $t'_p > t'_b$. In (a), thinning of the layer is measured from the right-hand side of the finite-element mesh at times extrapolated to the time when the blob should have dropped to infinite depth. These measurements show that for most runs $\Delta h \approx 0.7$–$0.9h$ for an inviscid underlying half-space, and $\Delta h \approx 1.2h$ for a viscous substrate. In (b), theoretical calculations of $\Delta h/L$ using eq. (23) are plotted against t'_p on a logarithmic scale using $n = 3$ and $C_{L\Delta\rho} = 0.75$, estimated from Fig. 9.

way and summed:

$$t_p \approx t_b + \frac{1}{(n-1)} \left(\frac{nB_0}{C_{L\Delta\rho} g \Delta\rho L} \right)^n \sum_{j=1}^{p-1} e^{jn}. \tag{21}$$

The summation assumes p is an integer, but it may be approximated by an integral in order to allow any real $p > 1$:

$$t_p \approx \frac{1}{(n-1)} \left(\frac{nB_0}{C_{L\Delta\rho} g \Delta\rho L} \right)^n \left[\left(\frac{Z_0}{L} \right)^{1-n} + \frac{e^{n/2}}{n} (e^{(p-1)n} - 1) \right], \tag{22}$$

and this equation can be inverted for $t_p > t_b$ and $L < \Delta h < h$ to give the approximate thickness of lithosphere removed in time $t'_p = t_p(g\Delta\rho L/B_0)^n$:

$$\frac{\Delta h}{L} \approx 1 + \frac{1}{n} \ln \left\{ 1 + ne^{-n/2} \left[\left(\frac{C_{L\Delta\rho}}{n} \right)^n (n-1)t'_p - \left(\frac{Z_0}{L} \right)^{1-n} \right] \right\}. \tag{23}$$

The logarithmic dependence on time in eq. (23) shows that the rate at which the layer is thinned decreases with increasing time (Fig. 11b). The time required to remove the lowest part of the lithosphere ($\Delta h \approx L$) decreases rapidly as the amplitude of the initial perturbation Z_0/L increases, but further thinning ($\Delta h > \sim 3L$) is so much slower that the total elapsed time is insensitive to the time required for the initial instability (Fig. 11b). The derivation of eq. (23) neglects a geometric factor of order 1, which could change the slope of the line shown in Fig. 11(b). Except, however, for the neglect of conduction of heat, which limits the applicability of eq. (23) to the lithosphere, the form of its time dependence should be robust.

5 INSTABILITY OF A NON-NEWTONIAN LAYER DURING HORIZONTAL SHORTENING

Most mountain ranges are built by crustal thickening due to crustal shortening, and that shortening not only can create an instability at the base of the lithosphere, but also could affect the viscosity structure of the straining lithosphere. If the entire lithosphere undergoes such shortening, and if it behaves like a fluid with non-linear viscosity, such shortening should impose a non-negligible background strain rate that will reduce the effective viscosity of the lithosphere. If shortening occurs at an approximately constant rate, it sets a constant value to the second invariant of the strain rate tensor. With this background viscosity structure, a Rayleigh–Taylor instability should initially grow exponentially (e.g. Conrad & Molnar 1997) with a growth rate given by eq. (1), but with a viscosity given by eq. (3). The dimensionless growth rate depends on the exponent n relating stress and strain rate. Thus, for linearly decreasing density and constant B, which we consider first here, $q'_h(kh, r, n)$ reaches a maximum near $kh \sim 1$ (Conrad & Molnar 1997). In principle, when the perturbation grows sufficiently, and strain rates due to the instability exceed the background strain rate, the non-linear dependence of viscosity on strain rate should cause the growth to become super-exponential, as in eqs (4) and (5).

We carried out experiments with a layer undergoing shortening in order both to verify that growth would initially be exponential, and to examine the transition from exponential growth appropriate to a constant background strain rate to super-exponential growth. We first considered a layer of constant rheological parameter $B = B_0$, and then a layer with a viscosity coefficient decreasing exponentially in the layer (eq. 10). In both cases, we used a layer with $n = 3$ and with density decreasing linearly with depth, overlying an inviscid half-space. We imposed shortening by moving the right-hand side of the layer at a constant rate u_0 towards the left and by imposing a constant horizontal displacement rate to the top of the layer at $z = h$ proportional to the distance from the left edge:

$$u(x) = -2u_0 x/\lambda, \quad 0 \leq x \leq \lambda/2, \quad z = h. \tag{24}$$

We then set the dimensionless rate such that super-exponential growth would begin before the amount of shortening of the layer reached a significant fraction of λ. The two stages of growth described above imply that there are two natural timescales for these experiments. For the initial stage, we analyze these experiments using a timescale that depends on the convergence rate and is best for describing the exponential

growth stage. We then rescale the same data using the timescale of (eq. 16), which is independent of the convergence rate and is best for analysis of the super-exponential growth stage.

5.1 Constant rheological parameter B

We carried out many experiments before discovering a combination of parameters that allowed exponential growth initially but also permitted super-exponential growth to begin before the layer had shortened by tens of per cent, which would affect the wavelength of the instability. Because of the assumption of incompressibility of the layer, shortening it imposes a downward speed and displacement on the base of the layer (due to uniform thickening). To estimate the growth of the instability, therefore, we corrected the speeds and positions of the lower left corner of the layer by the following:

$$w_{\text{corr}} = w + \frac{2u_0 h\lambda}{(\lambda - 2u_0 t)^2}, \tag{25}$$

$$Z_{\text{corr}} = Z + \frac{2hu_0 t}{(\lambda - 2u_0 t)^2}. \tag{26}$$

The corrections are positive because both w and Z are negative for the lower left corner of the layer and u_0 is treated as positive here. If the background perturbation is small, we may assume that the strain rate is uniform, $\dot{E} = \dot{\varepsilon}_{xx} = 2u_0/\lambda$ and the constant background viscosity from eq. (3) is

$$\eta_{hs} = \frac{B}{2}\left(\frac{2u_0}{\lambda}\right)^{(1-n)/n}. \tag{27}$$

We rendered time dimensionless using a timescale based on eq. (1) and the background viscosity (eq. 27):

$$T_{hs} = \left(\frac{B}{g\beta h^2}\right)\left(\frac{2u_0}{\lambda}\right)^{(1-n)/n}, \tag{28}$$

and rendered distance dimensionless using h. The subscript 's' indicates shortening. We plotted $\ln w''_{\text{corr}}$ and $\ln Z''_{\text{corr}}$ versus t'' (Fig. 12), and we measured the growth rates q''_h from the slopes of the linear segments for small values of t''. (We use double primes to distinguish non-dimensionalization using eq. (28) in place of eq. (16), although $Z'' = Z'$.)

For small initial perturbations of $Z_0 = 0.001h$ or $0.0001h$ in eq. (13), and for sufficiently rapid shortening rates, initial growth is exponential (Fig. 12). Moreover, the experimental growth rates q''_h agree within a few per cent with those predicted theoretically by Conrad & Molnar (1997) (Fig. 13). This agreement demonstrates that shortening, by imposing a higher strain rate than is caused by the growth of the instability, causes the layer to behave as if its viscosity is constant and relatively low.

This agreement, however, holds only for $Z_0 \ll 0.01h$. For initial perturbations of $Z_0 = 0.01h$, which hardly seem large, but nevertheless are much larger than those used for the results that match the theory (Figs 12 and 13), we estimated exponential growth rates that differ by tens of per cent from those with smaller perturbations (Fig. 12). When the perturbation is small ($Z_0 \leq 0.001h$), initially the only deformation of the layer is due to shortening and thickening of it at a constant strain rate; therefore the viscosity throughout the layer is nearly constant. For runs with the larger perturbations ($Z_0 = 0.01h$), however, the instability grows sufficiently rapidly that strain rates vary through the layer. On the left-hand side,
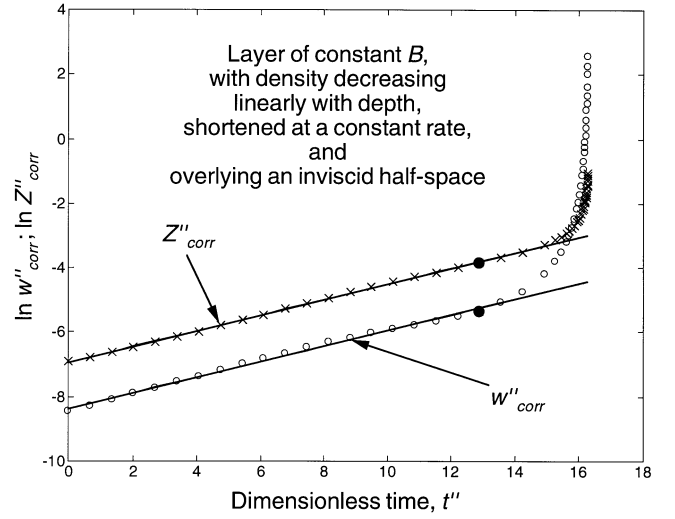

Figure 12. Plots of $\ln w''_{\text{corr}}$ and $\ln Z''_{\text{corr}}$ versus t'' for a layer with density decreasing linearly with depth, with constant rheological parameter B and with $n = 3$ in eq. (3), where the layer shortens at a constant speed u''_0 ($= u_0 T_{hs}/h) = 3.68 \times 10^{-3}$. The layer overlies an inviscid half-space. The linearity of the initial data (bounded by the filled circles) defines the initial growth rate $q''_h = qT_{hs}$, where T_{hs} is defined by eq. (28).
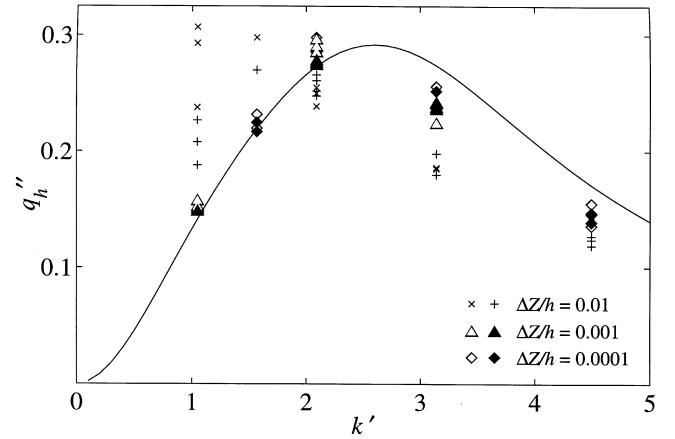

Figure 13. Plot of growth rates q''_h versus wavenumber $k' = kh$, determined from finite-element calculations (symbols) and from linearized calculations (lines), for a layer with density decreasing linearly, with constant rheological parameter B and with $n = 3$ in eq. (3), where the layer shortens at constant speed. The layer overlies an inviscid half-space. Open and solid symbols as in Fig. 4. Note that for cases with small initial perturbations of $Z_0 = 0.001h$ (triangles) or $0.0001h$ (diamonds) in eq. (13), the calculated and theoretical growth rates q''_h agree, but for larger initial perturbations ($\times$ or $+$), they do not. The basic assumptions of the linearized calculations are invalid when the initial perturbations are too large.

where both shortening and growth of the instability combine to cause the bottom of the layer to move downward, high strain rates make the viscosity relatively small. On the right-hand side, however, the instability causes the right-hand side to thin, but shortening causes it to thicken. Thus, the right-hand side behaves like a stagnant, non-deforming region, and the low strain rates make the viscosity there large.

These spatial variations in strain rate result in variations in viscosity that shorten the effective length of the deforming

region and make the instability become localized where the viscosity is lowest. For a length of the layer corresponding to wavelengths and wavenumbers near those appropriate for maximum growth rate ($k' \sim k'_{max}$), the reduction in the effective length of the deforming region makes the effective wavenumber larger than that for maximum growth rate: $k' > k'_{max}$. Thus, measured growth rates for large perturbations are less than those for small perturbations, for which the entire width of the layer is involved in the instability. For the largest wavelength that we studied ($\lambda = 6h$) and therefore the smallest wavenumber, $k' = 1.05$, however, reducing the effective length of the layer allows an instability with k' closer to k'_{max} to grow; hence the growth rate for a large perturbation is greater than that for a small perturbation (Fig. 13).

Following a period of initial exponential growth, after the base of the layer has deformed sufficiently, growth becomes super-exponential. We rescaled the output of the previous experiments so that time is now rendered dimensionless by $T_{h\beta} = (B/g\beta h^2)^n$, analogous to eq. (16); distance is rendered dimensionless by h, and speed by $h/T_{h\beta}$. Fitting the values of w'_{corr} and Z'_{corr} in eqs (25) and (26) to curves of the form of eqs (4) and (5) again yields straight lines (Fig. 14), with values of $C_{h\beta}$ (Fig. 15) similar to those obtained for layers without imposed horizontal shortening. Houseman & Molnar (1997) obtained* $C_{h\beta} \approx 0.47$ at $kh = 2.09$. The values of $C_{h\beta}$ are independent of the shortening rate, as expected for this stage in development, where growth is rapid compared to the shortening rate. Growth consists of two stages that obey simple
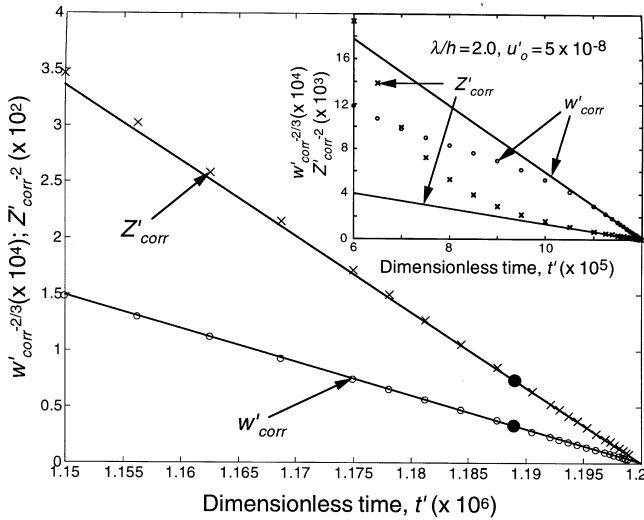

Figure 15. Plot of measured values of $C_{h\beta}$ versus k' for a layer with density decreasing linearly with depth, with constant rheological parameter B, where horizontal shortening of the layer occurs at a constant rate.

rules describing the development of the instability with time, which are separated by a third, brief transition stage.

The transition from initially exponential to later super-exponential growth requires a finite time, but we may approximate it as abrupt. For the initial, exponential growth (eq. 1) of both downward speed and position,

$$w(t) = qZ(t) = \left[\left(\frac{g\beta h^2}{B} \right) \left(\frac{2u_0}{\lambda} \right)^{(n-1)/n} q''_h(kh) \right] Z(t), \qquad (29)$$

where q is obtained from eqs (28) and (1). Later, in the super-exponential phase, from eqs (4) and (5) (using βh in place of $\Delta\rho$),

$$w(t) = h \left(C_{h\beta}(kh) \frac{g\beta h}{nB} Z(t) \right)^n. \qquad (30)$$

Thus, from eqs (29) and (30), the transition should occur at the following dimensional values of w and Z:

$$Z_t = \left(\frac{B}{g\beta h} \right) \left(\frac{n}{C_{h\beta}} \right)^{n/(n-1)} \left(\frac{2u_0}{\lambda} \right)^{1/n} q''^{1/(n-1)}_h, \qquad (31)$$

$$w_t = h \left(\frac{2u_0}{\lambda} \right) \left(\frac{nq''_h}{C_{h\beta}} \right)^{n/(n-1)}. \qquad (32)$$

We may test these relationships by plotting $\ln w'_{corr}$ versus $\ln Z'_{corr}$ (Fig. 16). As expected, for the initial stage when growth is exponential, $\ln w'_{corr}$ and $\ln Z'_{corr}$ vary linearly with one another. For the later, super-exponential stage, the slope of $\ln w'_{corr}$ versus $\ln Z'_{corr}$ is 3, as it should be from eq. (30). The final super-exponential stages are virtually identical, showing no dependence on the rate of shortening. The initial exponential phases, however, clearly do depend on that rate; with faster shortening, and therefore lower viscosity, initial speeds are higher. Moreover, the transition from exponential to super-exponential growth occurs for a larger growth of the perturbation to the boundary, as seen in eq. (31). Such linearity for the two branches is clearest for runs that examine wavenumbers close to k'_{max}.

Given an initial displacement Z_0, we can now compute the approximate time interval t_b required for removal of the lower part of the layer. This interval consists of two terms,

Figure 14. Plots of Z'^{1-n}_{corr} and $w'^{1/n-1}_{corr}$ versus t', with times non-dimensionalized by eq. (16), but with $\beta h = \Delta\rho$, for a layer with density decreasing linearly with depth, with constant rheological parameter B and with $n = 3$, where the layer undergoes horizontal shortening at a constant speed of u'_0 ($= u_0 T_{h\beta}/h$) $= 5 \times 10^{-8}$. In the inset, part of the exponential growth is shown (here as a decay because of the negative power), but near $t' = 11 \times 10^5$, super-exponential growth takes over. For the largest values of t', indicated by the filled circles, the linear fits of Z'^{1-n}_{corr} and $w'^{1/n-1}_{corr}$ versus t' demonstrate super-exponential growth, with straight lines used to define the values of $C_{h\beta}$.

* Houseman & Molnar (1997) (p. 144) in fact obtained $C_{h\beta} \approx 0.94$, but because their non-dimensionalization of density differs by a factor of 2 from ours, so does their definition of $C_{h\beta}$.
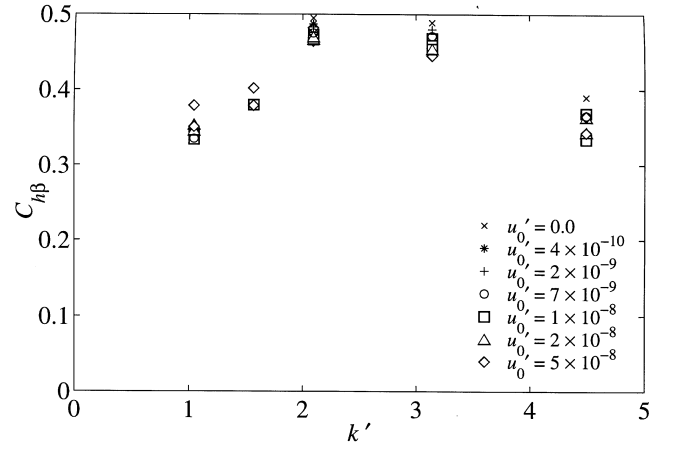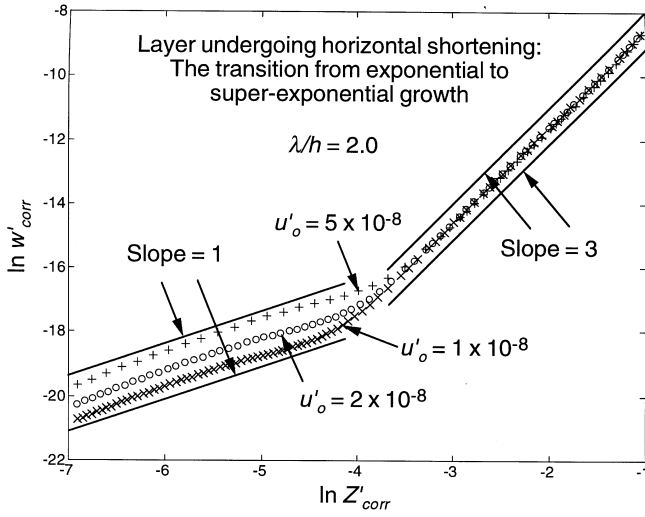
Figure 16. Plots of $\ln w'_{corr}$ versus $\ln Z'_{corr}$ for a layer with density decreasing linearly with depth, with constant B, where horizontal shortening of the layer occurs at a constant rate: $\times$ $u'_0(=u_0 T_{h\beta}/h) = 1 \times 10^{-8}$; $\bigcirc$ $u'_0 = 2 \times 10^{-8}$; $+$ $u'_0 = 5 \times 10^{-8}$. The layer overlies an inviscid half-space. Notice that for small w'_{corr} and Z'_{corr}, when growth is exponential, w'_{corr} and Z'_{corr} are proportional, but then a transition to super-exponential growth occurs, where w'_{corr} is proportional to the cube of Z'_{corr}. When the background strain rate is highest ($+$) and viscosity is lowest, exponential growth is most rapid and proceeds further before super-exponential growth takes over.

$t_1 = q^{-1}\ln(Z_t/Z_0)$ describing the interval of exponential growth from Z_0 to the transition amplitude Z_t (eq. 31), plus t_{nl} describing the interval of non-linear power-law growth from Z_t to completion of the instability [with Z_t from eq. (31) used in place of Z_0 in eq. (6)]:

$$t_b = t_1 + t_{nl} = \frac{1}{q''_h}\left(\frac{B}{g\beta h^2}\right)\left(\frac{2u_0}{\lambda}\right)^{(1-n)/n}\left[\frac{1}{(n-1)} + \ln\left(\frac{Z_t}{Z_0}\right)\right]. \tag{33}$$

5.2 Rheological parameter B varying exponentially with depth in the layer

Above, in Section 4, we showed that the same relationships that had worked for a layer of constant rheological parameter B (Houseman & Molnar 1997) also worked for B decreasing exponentially with depth in the layer, provided only that we use the length scale L in place of h. The differences manifest themselves as different dimensionless constants C (whose interrelationships are shown in Table 3). Here we again test whether the same basic rules shown to apply to a layer with a constant rheological parameter—those that describe an initial exponential growth (eq. 1) and a final super-exponential growth (eqs 4 and 5)—also apply to the case where the rheological parameter B decreases exponentially with depth to B_0 at $z' = 0$.

We define a time unit $T_{Ls} = (B_0/\beta g L^2)(2u_0/\lambda)^{1/n-1}$ using eq. (28), with L in place of h to render distance dimensionless. Plots of $\ln w''_{corr}$ and $\ln Z''_{corr}$ versus t'', with corrections to w'' and Z'' again made as in eqs (25) and (26), yield straight lines, showing that the initial growth is exponential. The measured dimensionless growth rates q''_L are essentially independent of the rates of shortening and depend only weakly on the ratio
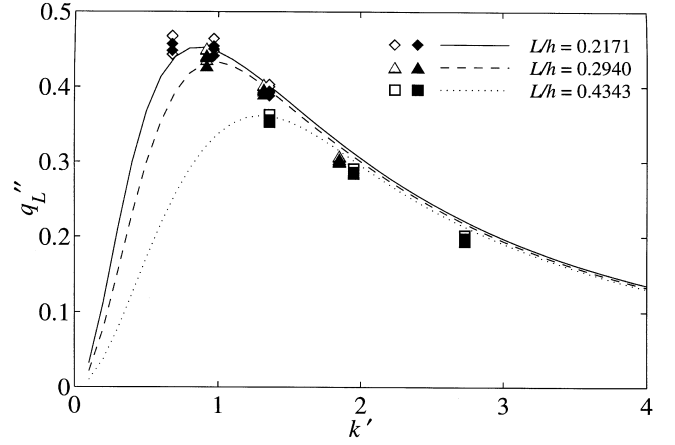

Figure 17. Plot of growth rates $q''_L = qT_{Ls}$ (Table 2), measured from experiments (symbols) and from linearized calculations (lines), versus wavenumber $k' = kL$, for a layer undergoing shortening at a constant rate, with density decreasing linearly in the layer, and with the rheological parameter B decreasing exponentially with depth. The layer overlies an inviscid half-space. Open and solid symbols as in Fig. 4.
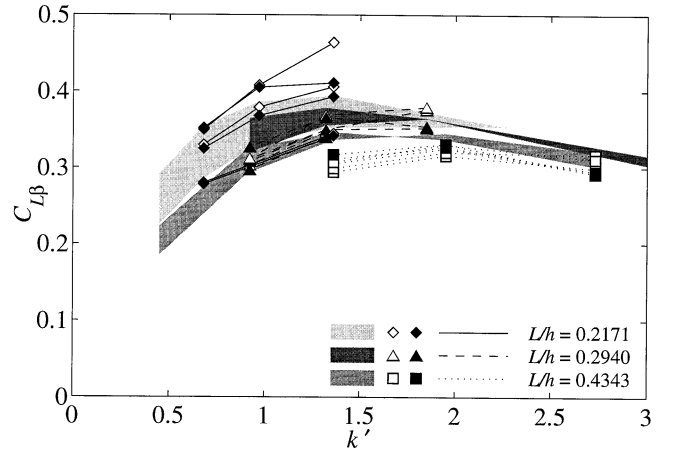

Figure 18. Plot of measured values of $C_{L\beta}$ versus k', for a layer with density decreasing linearly and with the rheological parameter B decreasing exponentially with depth, where horizontal shortening of the layer occurs at a constant rate. The shading shows results from runs without horizontal shortening (Fig. 10).

L/h, as calculated from linear theory following the same procedures as used by Conrad & Molnar (1997) (Fig. 17). To analyse the final stages of growth in these experiments, we rescaled the output so that distance is again rendered dimensionless by L but time is now rendered dimensionless using $T_{L\beta}$ (Table 2), and speed using $L/T_{L\beta}$. Plots of Z'^{1-n}_{corr} and $w'^{(1/n-1)}_{corr}$ versus t' for the final stages of growth also obey forms like eqs (18) and (19) or eqs (4) and (5). Moreover, most values of $C_{L\beta}$ as a function of k' (Fig. 18) agree within about 10 per cent with those obtained for layers that did not undergo shortening.

The initial exponential phase followed by a super-exponential phase obeying a form like eqs (18) and (19) implies that the relationships between w and Z in eqs (29)–(30) should apply again, but, of course, with h replaced by L, and with the appropriate values of q''_L (Fig. 17) and $C_{L\beta}$ (Fig. 18) used in them. Plots of $\ln w'_{corr}$ versus $\ln Z'_{corr}$ again show clearly

the transition from exponential growth to power-law growth, although for runs with a viscosity variation of 100 times ($L = 0.2171h$), the super-exponential phase is not matched precisely by the simplified theory. The amplitude at which the transition occurs is now

$$Z_{tL} = \left(\frac{B_0}{g\beta L}\right)\left(\frac{n}{C_{L\beta}}\right)^{n/(n-1)}\left(\frac{2u_0}{\lambda}\right)^{1/n} q_L''^{1/(n-1)}. \tag{34}$$

6 APPLICATION TO THE EARTH

Below, we apply the results given above to the Earth. To do so, we must first choose values for the relevant parameters B_0, n, g, β and L. For the Earth, $g = 9.8 \text{ m s}^{-2}$.

Assuming that only temperature affects the density, we must assume a temperature gradient to estimate β. For lithosphere with 35 km of crust, with a temperature $\theta = 800$ K at the Moho and $\theta = 1600$ K at the base of the lithosphere 100 km deeper, $d\theta/dz = -8 \text{ K km}^{-1}$. For a lithosphere twice as thick, either initially or after thickening by two times, $d\theta/dz = -4 \text{ K km}^{-1}$. With the density gradient given by $d\rho/dz = -\alpha\rho(d\theta/dz)$, with $\alpha = 3 \times 10^{-5} \text{ K}^{-1}$ and $\rho = 3.35 \times 10^3 \text{ kg m}^{-3}$, $\beta = 8 \times 10^{-4} \text{ kg m}^{-4}$ or $4 \times 10^{-4} \text{ kg m}^{-4}$ for these two temperature gradients.

We use laboratory measurements of the temperature dependence of deformation of olivine (e.g. Goetze 1978; Karato, Paterson & Fitzgerald 1986) to constrain the rheological parameter B appropriate to the mantle and necessary for evaluating L. In Appendix A, we derive the relationship between deviatoric stress and strain rate appropriate to such measurements:

$$B = 3^{-(n+1)/2n}\left(\frac{A}{2}\right)^{-1/n}\exp\left(\frac{H}{nR\theta}\right), \tag{35}$$

where A is an experimentally determined constant, H is the activation enthalpy, R is the universal gas constant ($= 8.3 \text{ J K}^{-1} \text{ mole}^{-1}$) and the numerical constant arises from using second invariants of the stress and strain rate tensors to express the laboratory measurements (see Appendix A). Karato *et al.* (1986) gave, for dry olivine, $n = 3.5$, $A = 2.4 \times 10^5 \text{ s}^{-1} \text{ MPa}^{-3.5}$ and $H = 540 \text{ kJ mole}^{-1}$ and, for wet olivine, $n = 3$, $A = 1.9 \times 10^3 \text{ s}^{-1} \text{ MPa}^{-3}$ and $H = 420 \text{ kJ mole}^{-1}$. To estimate L, we may approximate eq. (35) by

$$B = 3^{-(n+1)/2n}\left(\frac{A}{2}\right)^{-1/n}\exp\left(\frac{H}{nR[\theta_0 + (d\theta/dz)z]}\right), \tag{36}$$

where $d\theta/dz$ is the temperature gradient in the lithosphere. We may approximate eq. (36) by

$$B \approx B_0 \exp\left(\frac{-H(d\theta/dz)z}{nR\theta_0^2}\right), \tag{37}$$

which, from eq. (10), implies that

$$L \approx -\frac{nR\theta_0^2}{H(d\theta/dz)} \tag{38}$$

and

$$B_0 = 3^{-(n+1)/2n}\left(\frac{A}{2}\right)^{-1/n}\exp\left(\frac{H}{nRT_0}\right). \tag{39}$$

To estimate L, let us choose $\theta_0 = 1323$ K (1050 °C), a temperature in the lower lithosphere within the interior of the area

we expect to be unstable. Using the parameters given above and the steeper temperature gradient (8 K km^{-1}), $L = 12$ km for dry olivine, and $L = 13$ km for wet olivine. The values of L for the 4 K km^{-1} temperature gradient are twice as large. [For the parameters given by Hirth & Kohlstedt (1996), the values for dry olivine give $L = 12$ and 24 km, and those for wet olivine give $L = 12$ and 25 km.]

6.1 Thickness of lower lithosphere removed by the instability

The value of B decreases by several orders of magnitude through the lithosphere. Yet, several studies of convection in a medium with temperature-dependent viscosity show that only a portion across which the viscosity varies by 10 to 100 times is vigorously involved in the convection (e.g. Buck & Toksöz 1983; Fleitout & Yuen 1984; Jaupart & Parsons 1985; Moresi & Solomatov 1995; Yuen & Fleitout 1984). The remaining upper, colder part is nearly stagnant. Presumably, during steady-state convection, only this basal, lowest-viscosity part of the lithosphere participates.

Mechanical thickening of the lithosphere, however, should increase the thickness of the layer that is unstable. Our experiments have considered a range of B that spans only a factor of 100 and therefore might seem to address only the bottommost part of the lithosphere. Note, however, that for $n = 3$ (at a constant stress level), a variation in B by a factor of 100 causes a range of $\sim 10^6$ in the effective viscosity across the layer. Recall also that these experiments considered cases in which the unstable layer is underlain by either an inviscid half-space or a viscous layer assigned the same value of B as that at the base of the layer (Fig. 19). Thus, these experiments can be used to bound the growth of unstable portions of mantle lithosphere where the viscosity exceeds that of the asthenosphere by factors much greater than 100. In any case there is every indication that the asymptotic scaling that we have found is valid for all L less than about h.

Houseman & Molnar (1997) showed that, for a layer with constant properties, the dimensionless time t_b' for a blob of material to drop off the rest of the layer could be related to the dimensionless initial perturbation of the bottom, Z_0', by

$$t_b' = \left(\frac{n}{C}\right)^n \frac{Z_0'^{(1-n)}}{(n-1)}. \tag{40}$$

The experiments described above verify that the equations used to derive eq. (40) apply also to cases where the viscosity decreases exponentially with depth and the density decreases linearly with depth in the layer. Thus, we may employ the dimensional form of eq. (40), with eq. (14) to dimensionalize distance and eq. (16) for time:

$$t_b = \left(\frac{nB_0}{C_{\beta L}g\beta L^2}\right)^n \frac{(Z_0/L)^{1-n}}{n-1}. \tag{41}$$

This provides a relationship between the initial perturbation and the time that must elapse for removal of the base of the layer. Note that if (1) we assume the flow parameters for wet olivine, (2) we use the value of $C_{\beta L} = 0.3$ appropriate to a layer over a viscous half-space (Fig. 10), (3) we associate B_0 with the base of the lithosphere, where $\theta = 1623$ K (for which $B_0 = 800 \text{ MPa s}^{1/3}$) and (4) we assume a perturbation of magnitude $Z_0 \sim L$ to the base of the lithosphere, then a thickness
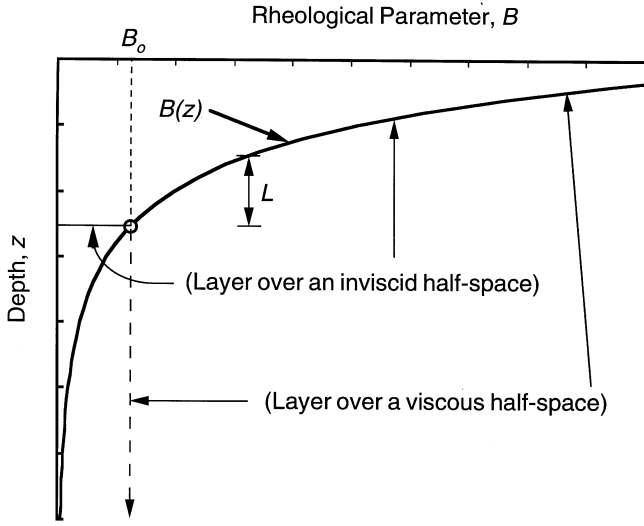
Rheological Parameter, *B*

Figure 19. Plot of rheological parameter *B* versus depth *z*, and its relationship to the values of B_0 and *L* used in our experiments. *B* decreases continuously with depth through the lithosphere. We carried out experiments with layers in which *B* decreases exponentially with depth, over an inviscid half-space and over a viscous half-space in which *B* is constant and equal to the value at the base of the layer. These two states bound the realistic case in which *B* decreases continuously with depth. For an increased duration of time, a layer of increased thickness should become unstable. Thus we seek a value of B_0 appropriate to the base of an unstable layer that grows in a specified amount of time. Then from the corresponding inferred temperature and depth, we estimate the thickness of material, both above and below the depth associated with B_0, that would be removed in the specified time.

$\sim L$ ($= 24$ km) of the basal lithosphere would be removed in a geological instant, $t_b = 600$ yr! Obviously, a much thicker layer will be removed during the period typically required for lithospheric thickening.

The short timescale for the initial instability in a stratified layer whose strength parameter decreases with depth, coupled with the relatively thin layer removed by the initial instability, has been used previously to argue that convective thinning of thickened lithosphere would have little effect on the thermal structure of the lithosphere (Buck & Toksöz 1983). This argument is misleading, however, because the lithosphere continues to be thinned (at a decreasing rate) long after the initial instability. Our experiments were limited to the period that describes the initial instability (Fig. 11a), which we extrapolated to obtain an approximate theory that describes the timescale by which succeeding, higher-viscosity layers of the lithosphere are removed (Fig. 11b). A simple way to estimate the total thickness removed in a given time period follows from the assumption that most of the period is occupied by the removal of the uppermost, most viscous part of the layer that is removed. We take this approach and invert eq. (41) to evaluate the value of B_0 appropriate to a hypothesized time t_b for removal of this uppermost sublayer:

$$B_0 = \frac{C_{\beta L} g \beta L u}{n} \sqrt[n]{(n-1) t_b L Z_0^{n-1}} . \tag{42}$$

Then, from an estimate of B_0 appropriate to an assumed time t_b, we use eq. (39) to estimate the corresponding temperature and thickness of the layer removed.

Let us suppose that the entire lithosphere was thickened to twice its normal value, letting $Z_0 = 100$ km, and that the temperature gradient was halved from 8 K km^{-1} to 4 K km^{-1}. From Fig. 10, we use $C_{\beta L} = 0.35$, appropriate to wet olivine, for which $n = 3$. Houseman & Molnar (1997) showed that for constant density and rheological parameter in the layer, *C* depends weakly on *n*; assuming a similar variation for the cases considered above, we use $C_{\beta L} = 0.45$ for dry olivine, for which $n = 3.5$ (e.g. Hirth & Kohlstedt 1996). Let us consider the thickness that would be removed after 10 Myr. With $L = 24$ km or 25 km, appropriate to dry or wet olivine, we estimate from eq. (42) $B_0 = 1.5 \times 10^{10}$ Pa s$^{1/3.5}$ or $B_0 = 6.0 \times 10^{10}$ Pa s$^{1/3}$ respectively. From eq. (35), these values of B_0 imply values of temperature of 1361 K (1088 °C) and 1203 K (930 °C) respectively. Recognizing that material of thickness $\sim L$ above this level is removed (Fig. 11a), these temperatures underestimate the amount of lithosphere convectively removed. Additional thicknesses of $\sim L$ correspond to material ~ 100 K colder than that deduced from B_0. Thus, assuming that Rayleigh–Taylor instability applies to these two cases, we expect that for dry olivine, material colder than the asthenosphere by ~ 400 K, and for wet olivine, material colder by ~ 500 K would be removed. With a gradient of 4 K km^{-1}, such temperature contrasts correspond to thicknesses ranging from ~ 100 to 125 km of mantle lithosphere, previously thickened to ~ 200 km. Thus, they permit convective removal of somewhat more than half of the lithosphere, but not the entire mantle lithosphere. These estimates of the thickness of lithosphere that may be involved in a convective thinning event do not greatly differ from those of Houseman & Molnar (1997), who based their estimates on the behaviour of an unstable layer whose rheological parameter is constant.

6.2 Growth of the perturbation during shortening

We arbitrarily chose a doubling of the thickness of the lithosphere by mechanical processes, but if shortening occurs, the super-exponential phase should be preceded by an exponential phase. Eq. (31) relates the magnitude of the layer thickness perturbation that develops before super-exponential growth sets in to the rheological parameters, and to the background strain rate. Rendering eq. (31) appropriate to exponential variation of the rheological parameter yields

$$Z_t = \left(\frac{B_0}{\beta g L}\right)\left(\frac{n}{C_{\beta L}}\right)^{n/(n-1)}\left(\frac{2u_0}{\lambda}\right)^{1/n} q_L''^{1/(n-1)} . \tag{43}$$

To evaluate eq. (43), let us use the estimates of B_0 obtained above for dry and wet olivine (1.5×10^{10} Pa s$^{1/3.5}$ and 6.0×10^{10} Pa s$^{1/3}$ respectively). Let us assume that shortening occurs at a rate of 100 per cent in 20 Myr, corresponding to $\dot{E} = 2u_0/\lambda = 1.58 \times 10^{-15}$ s^{-1}. With $q_L'' = 0.35$, we obtain $Z_t = 107$ km for dry olivine and 108 km for wet olivine. As these values of Z_t depend weakly on the background strain rate (on its *n*th root), more or less rapid straining will not affect the amounts much. The linear dependences on B_0 and on the product βL govern the uncertainty in Z_t. In any case, the magnitude of the values obtained suggests that the layer is likely to develop major thickness perturbations during the exponential phase of growth associated with crustal shortening.

6.3 Summary of applications to the Earth

First, we emphasize that the main goal of this study has not been to model the Earth, but rather to obtain an understanding of how specific structural conditions and processes appropriate to the Earth might affect the gravitational instability of an unstable viscous layer such as the Earth's lithosphere. These conditions include non-linear relations between stress and strain rate, an exponentially decreasing rheological parameter, a linearly decreasing density and an externally imposed horizontal shortening of the layer. The main results are expressed in algebraic equations that relate times, rates and amounts of growth of perturbations to the material parameters.

The application of these equations to the Earth suggests that for a timescale of approximately 20 Myr, during which the lithosphere in zones of rapid crustal shortening will be mechanically thickened by roughly two times, exponential growth will cause perturbations of the base of the lithosphere to grow to amplitudes of the order of 100 km. Then, in a subsequent period of comparable length (~ 20 Myr), complete removal of a layer of lower lithosphere, also of the order of 100 km thick, can occur for rheological parameters and other assumptions appropriate to the lithosphere in zones of active convergence. These calculations corroborate those of Houseman & Molnar (1997) in suggesting that half or more (though probably not all) of the mantle lithosphere may be removed by the convective thinning process following convergent orogeny. Because we ignored lateral conduction of heat in analysing Rayleigh–Taylor instability, the thicknesses of material removed might be overestimated (and the times for convective thinning might be underestimated) here (e.g. Conrad & Molnar 1997). The effect of thermal conduction on these estimates is essentially a correction, reducing growth rates in the stage of exponential growth but, on these timescales of 20–40 Myr, not changing the basic pattern of the process that we have described here.

REFERENCES

Bassi, G. & Bonnin, J., 1988. Rheological modelling and deformation instability of lithosphere under extension, *Geophys. J.,* **93,** 485–504.

Buck, W.R. & Toksöz, M.N., 1983. Thermal effects of continental collisions: thickening a variable viscosity lithosphere, *Tectonophysics,* **100,** 53–69.

Canright, D. & Morris, S., 1993. Buoyant instability of a viscous film over a passive fluid, *J. Fluid Mech.,* **255,** 340–372.

Chandrasekhar, S., 1961. *Hydrodynamic and Hydromagnetic Stability,* Oxford University Press, Oxford.

Conrad, C.P. & Molnar, P., 1997. The growth of Rayleigh–Taylor-type instabilities in the lithosphere for various rheological and density structures, *Geophys. J. Int.,* **129,** 95–112.

England, P.C. & Houseman, G.A., 1989. Extension during continental convergence, with application to the Tibetan Plateau, *J. geophys. Res.,* **94,** 17 561–17 579.

Fitton, J.G., James, D., Kempton, P.D., Ormerod, D.S. & Leeman, W.P., 1988. The role of lithospheric mantle in the generation of late Cenozoic basic magmas in the western United States, *J. Petrol., Spec. Lithosphere Issue,* 331–349.

Fleitout, L. & Yuen, D.A., 1984. Steady state, secondary convection beneath lithospheric plates with temperature- and pressure-dependent viscosity, *J. geophys. Res.,* **89,** 9227–9244.

Goetze, C., 1978. The mechanisms of creep in olivine, *Phil. Trans. R. Soc. Lond.,* A, **288,** 99–119.

Hirth, G. & Kohlstedt, D.L., 1996. Water in the oceanic upper mantle: implications for rheology, melt extraction and the evolution of the lithosphere, *Earth planet. Sci. Lett.,* **144,** 93–108.

Houseman, G.A. & Molnar, P., 1997. Gravitational (Rayleigh–Taylor) instability of a layer with non-linear viscosity and convective thinning of continental lithosphere, *Geophys. J. Int.,* **128,** 125–150.

Houseman, G.A., McKenzie, D.P. & Molnar, P., 1981. Convective instability of a thickened boundary layer and its relevance for the thermal evolution of continental convergent belts, *J. geophys. Res.,* **86,** 6115–6132.

Jaupart, C. & Parsons, B., 1985. Convective instabilities in a variable viscosity fluid cooled from above, *Phys. Earth planet. Inter.,* **39,** 14–32.

Jordan, T.H., 1975. The continental tectosphere, *Rev. Geophys. Space Phys.,* **13,** 1–12.

Karato, S.-I., Paterson, M.S. & FitzGerald, J.D., 1986. Rheology of synthetic olivine aggregates; influence of grain size and water, *J. geophys. Res.,* **91,** 8151–8176.

Lenardic, A. & Kaula, W.M., 1995. More thoughts on convergent crustal plateau formation and mantle dynamics with regard to Tibet, *J. geophys. Res.,* **100,** 15 193–15 203.

Molnar, P., England, P. & Martinod, J., 1993. Mantle dynamics, the uplift of the Tibetan Plateau, and the Indian monsoon, *Rev. Geophys.,* **31,** 357–396.

Moresi, L.-N. & Lenardic, A., 1997. Three-dimensional numerical simulations of crustal deformation and subcontinental mantle convection, *Earth planet. Sci. Lett.,* **150,** 233–243.

Moresi, L.-N. & Solomatov, V.S., 1995. Numerical investigation of 2D convection with extremely large viscosity variations, *Phys. Fluids,* **7,** 2154–2162.

Platt, J.P. & England, P.C., 1994. Convective removal of lithosphere beneath mountain belts: thermal and mechanical consequences, *Am. J. Sci.,* **294,** 307–336.

Turner, S., Arnaud, N., Liu, J., Rogers, N., Hawkesworth, C., Harris, N., Kelley, S., van Calsteren, P. & Deng, W., 1996. Post-collision, shoshonitic volcanism on the Tibetan Plateau: implications for convective thinning of the lithosphere and the source of ocean island basalts, *J. Petrol.,* **37,** 45–71.

Yuen, D.A. & Fleitout, L., 1984. Stability of the oceanic lithosphere with variable viscosity: an initial-value approach, *Phys. Earth planet. Inter.,* **34,** 173–185.

APPENDIX A: CONVERSION OF EXPERIMENTALLY DETERMINED RHEOLOGICAL PARAMETERS TO THOSE USED FOR VISCOUS FLOW

The experimentally measured deformation law is normally written in the form

$$\dot{\varepsilon}_{11} = A(\sigma_1 - \sigma_3)^n \exp\left(\frac{-H}{R\theta}\right), \tag{A1}$$

where the '1' direction is along the axis of compression, σ is the stress and A, H, R and θ are as defined in Table 1. Assuming incompressibility and symmetry,

$$\frac{1}{2}\dot{\varepsilon}_{11} = -\dot{\varepsilon}_{22} = -\dot{\varepsilon}_{33} \tag{A2}$$

and assuming isotropy,

$$\tau_{11} = -2\tau_{22} = -2\tau_{33}. \tag{A3}$$

Rewriting eq. (A1) in terms of deviatoric stress,

$$\dot{\varepsilon}_{11} = A(\tau_{11} - \tau_{33})^n \exp\left(\frac{-H}{R\theta}\right) = \left(\frac{3}{2}\right)^n A\tau_{11}^n \exp\left(\frac{-H}{R\theta}\right). \tag{A4}$$

Translating this into an expression invariant with respect to the definition of axes yields

$$\dot{\varepsilon}_{ij} = A'\vartheta^{n-1}\tau_{ij} \exp\left(\frac{-H}{R\theta}\right), \tag{A5}$$

where ϑ^2 is the second invariant of the deviatoric stress tensor. In the experimental measurements, shear stress components can be neglected, and the second invariant is then

$$\vartheta^2 = \frac{1}{2}(\tau_{11}^2 + \tau_{22}^2 + \tau_{33}^2) = \left(\frac{3}{4}\right)\tau_{11}^2. \tag{A6}$$

Expressing τ_{11} in terms of ϑ in eq. (A4) yields

$$\dot{\varepsilon}_{11} = \left(\frac{3}{2}\right)^n A\left(\frac{2}{\sqrt{3}}\vartheta\right)^{n-1}\tau_{11} \exp\left(\frac{-H}{R\theta}\right)$$

$$= \frac{3^{(n+1)/2}}{2}A\vartheta^{n-1}\tau_{11} \exp\left(\frac{-H}{R\theta}\right). \tag{A7}$$

Therefore, if eq. (A5) (for the general triaxial configuration) is to apply also to the experimental data (uniaxial compression), we require

$$A' = \frac{3^{(n+1)/2}}{2}A. \tag{A8}$$

We invert (A5) by squaring and summing over all components to get

$$\sum_{ij}\dot{\varepsilon}_{ij}\dot{\varepsilon}_{ij} = \sum_{ij}\tau_{ij}\tau_{ij}A'^2\vartheta^{2(n-1)} \exp\left(\frac{-2H}{R\theta}\right), \tag{A9}$$

which, using eq. (A6), gives an expression for the second invariant of the strain rate,

$$\dot{E} = A'\vartheta^n \exp\left(\frac{-H}{R\theta}\right), \tag{A10}$$

and hence, substituting for ϑ back into eq. (A5), we obtain

$$\tau_{ij} = A'^{-1/n}\dot{E}^{(1-n)/n}\dot{\varepsilon}_{ij} \exp\left(\frac{H}{nR\theta}\right). \tag{A11}$$

If we now write eq. (A11) in the usual form for use in viscous flow, given by eq. (2), we obtain

$$B = A'^{-1/n}\exp\left(\frac{H}{nR\theta}\right) = 3^{-(n+1)/2n}\left(\frac{A}{2}\right)^{-1/n}\exp\left(\frac{H}{nR\theta}\right). \tag{A12}$$